ARTICLES

Hedgehog regulates smoothened activity by inducing a conformational switch

Yun Zhao[1]*, Chao Tong[1]*† & Jin Jiang[1,2]

Hedgehog (HH) morphogen is essential for metazoan development. The seven-transmembrane protein smoothened (SMO) transduces the HH signal across the plasma membrane, but how SMO is activated remains poorly understood. In *Drosophila melanogaster*, HH induces phosphorylation at multiple Ser/Thr residues in the SMO carboxy-terminal cytoplasmic tail, leading to its cell surface accumulation and activation. Here we provide evidence that phosphorylation activates SMO by inducing a conformational switch. This occurs by antagonizing multiple Arg clusters in the SMO cytoplasmic tail. The Arg clusters inhibit SMO by blocking its cell surface expression and keeping it in an inactive conformation that is maintained by intramolecular electrostatic interactions. HH-induced phosphorylation disrupts the interaction, and induces a conformational switch and dimerization of SMO cytoplasmic tails, which is essential for pathway activation. Increasing the number of mutations in the Arg clusters progressively activates SMO. Hence, by employing multiple Arg clusters as inhibitory elements counteracted by differential phosphorylation, SMO acts as a rheostat to translate graded HH signals into distinct responses.

The HH morphogen controls many key development processes, with different thresholds specifying distinct outcomes[1–4]. In *Drosophila* wing discs, HH proteins secreted by posterior (P) compartment cells move into the anterior (A) compartment to form a local concentration gradient[5,6]. Low levels of HH suffice to induce the expression of *decapentaplegic* (*dpp*), whereas high levels are required to induce *patched* (*ptc*) and *engrailed* (*en*) (Supplementary Fig. 1)[7–9].

The reception system for HH consists of a twelve-transmembrane protein, PTC, as the HH receptor and a seven-transmembrane protein smoothened (SMO) as the signal transducer[10–13]. In *Drosophila*, HH binding to PTC abrogates its inhibition on SMO and induces extensive phosphorylation of the SMO cytoplasmic tail by protein kinase A (PKA) and casein kinase I (CKI), leading to SMO cell surface accumulation and activation[14–17]. How phosphorylation promotes SMO cell surface accumulation is not understood. In addition, phosphorylation may regulate SMO activity through mechanism(s) other than controlling its cell surface abundance.

Regulation of SMO by multiple Arg clusters

Our previous study indicates that phosphorylation may regulate SMO cell surface abundance by either preventing its endocytosis and/or promoting its recycling[15]. To investigate further how SMO cell surface expression is regulated, we generated a set of C-terminally truncated SMO variants and examined their subcellular localization using a cell-based assay (Fig. 1). Deletion up to amino acid 818 did not significantly change SMO subcellular distribution; however, further deletions resulted in progressively increased cell surface expression (Fig. 1a, c), implying that multiple negative regulatory elements exist between amino acids 661–818.

SMOΔC710 exhibits consistently higher cell surface expression than SMOΔC730 (Fig. 1c), indicating that amino acids 710–730 may harbour a negative element(s). Ala-scan mutagenesis, which substituted multiple residues to Ala, identified the Arg residues in RRTQRRR as critical for preventing SMO cell surface accumulation (Fig. 1b, c; data not shown). Interestingly, multiple Arg clusters, arbitrarily named R1 to R4, are located between amino acids 661–818, a region critical for blocking SMO cell surface accumulation (Fig. 1d). We therefore introduced into the full-length SMO Arg to Ala (RA) mutations in individual, or combinations of, Arg clusters. SMO variants with one Arg cluster mutated did not exhibit significant change in their cell surface expression; however, mutating two or more Arg clusters caused a gradual increase in SMO cell surface expression (Fig. 1d–f; data not shown), suggesting that multiple Arg clusters cooperate to restrict SMO cell surface accumulation.

To determine whether the Arg clusters negatively regulate SMO activity, SMO variants with one or more mutated Arg clusters were expressed in wing discs using the *MS1096 Gal4* driver. SMO variants with one mutated Arg cluster exhibited low levels of basal activity similar to that of wild-type SMO, as is evident from the ectopic expression of *dpp* but not *ptc* and *en* (Fig. 2a–c). However, SMO variants with two or more mutated Arg clusters exhibited a progressive increase in their constitutive signalling activities (Fig. 2d–i). Thus, SMO activity is inversely correlated with the number of functional Arg clusters. We also mutated several Arg clusters in the membrane-proximal region of the SMO cytoplasmic tail and observed no effect on SMO cell surface expression and activity (Supplementary Fig. 2). Hence, the Arg clusters between amino acids 661–818 are specifically involved in SMO autoinhibition.

Phosphorylation counteracts the Arg motifs

Increasing the number of phosphorylation-mimetic mutations in PKA/CKI sites resulted in a graded increase in SMO cell surface level and activity[15], which phenocopies the effect of increasing the number of RA mutations, indicating that phosphorylation may activate SMO by antagonizing the Arg motifs. Consistently, an internal deletion that removes both the phosphorylation and Arg clusters (SMOΔ661–818) results in high levels of SMO cell surface expression and activity (Figs 1a, c and 2j).

It is intriguing that the Arg clusters are situated adjacent to the PKA/CKI phosphorylation clusters (Fig. 1d). In fact, R1, R2 and R4

[1]Department of Developmental Biology, and [2]Department of Pharmacology, University of Texas Southwestern Medical Center, Dallas, Texas 75390, USA. †Present address: Department of Molecular and Human Genetics, Baylor College of Medicine, Houston, Texas 77030, USA.
*These authors contributed equally to this work.

are part of the PKA phosphorylation consensus site, R/KRXS. The juxtaposition of the Arg and phosphorylation clusters may allow precise control of SMO activity because phosphorylation at individual clusters may only neutralize the negative influence of adjacent Arg clusters. To test this, we constructed SMORA12D3 and found it behaved like SMORA124 (Fig. 1d, e; compare Fig. 2l with 2h), suggesting that phosphorylation at S3 (Fig. 1d) neutralizes the negative effect of R4.

Because Arg carries positive charge whereas phosphorylation brings in negative charge, phosphorylation may antagonize the Arg clusters by neutralizing their positive charges. In support of this model, we found that R3 and R4 can be functionally substituted by Lys, because SMORA12K34 behaved like SMORA12 rather than SMORA1234 (Fig. 1d, e, 2k). Furthermore, SMOEDS, which has three PKA/CKI phosphorylation clusters replaced by a stretch of acidic amino acids (Fig. 1d), exhibited high levels of cell surface expression and signalling activity similar to the phosphorylation-mimetic SMO variant, SMOSD123 (Fig. 1d, e, 2m; ref. 15), suggesting that the exact sequence composition of the phosphorylation clusters is not critical, but rather the negative charges they carry are important.

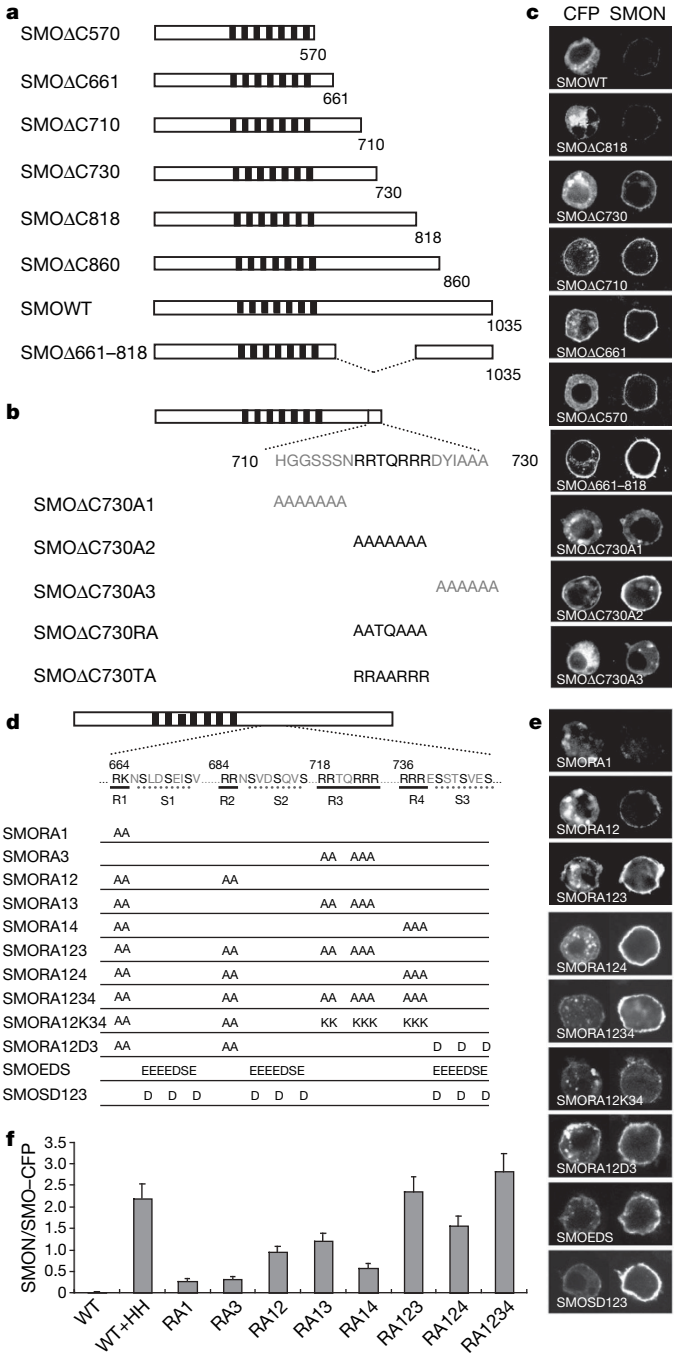

Figure 1 | Regulation of SMO cell surface expression by multiple Arg clusters. **a**, SMO deletion mutants with CFP (not shown) fused to their C termini. Filled boxes indicate the transmembrane domains. **b**, Ala-scan mutagenesis of SMOΔC730 with the last 20 amino acids and corresponding substitutions shown underneath. **c**, **e**, Cell surface expression of the indicated SMO mutants. S2 cells were transfected with the indicated CFP-tagged SMO constructs, followed by immunostaining with anti-SMON antibody before membrane permeabilization[15]. The SMON column indicates cell surface staining, whereas the CFP column indicates the total protein distribution. SMOΔ730RA and SMOΔ730TA behaved like SMOΔ710 and SMOΔ730, respectively (data not shown). **d**, A schematic drawing of a full-length SMO with the sequences of the four Arg clusters (R1–R4) and three phosphorylation clusters (S1–S3) shown underneath. SMO variants with the indicated substitutions are listed. **f**, Ratio of cell surface level (SMON signal) to total level (CFP signal) of protein for wild-type and indicated mutant forms of SMO. For SMO variants, $n = 20$; error bars, 1 s.d.

HH induces increased proximity of SMO cytoplasmic tails

Although SMO activity correlates with its cell surface levels, HH may induce SMO activation through additional mechanism(s) such as dimerization and/or conformational change[18,19]. To test these possibilities,

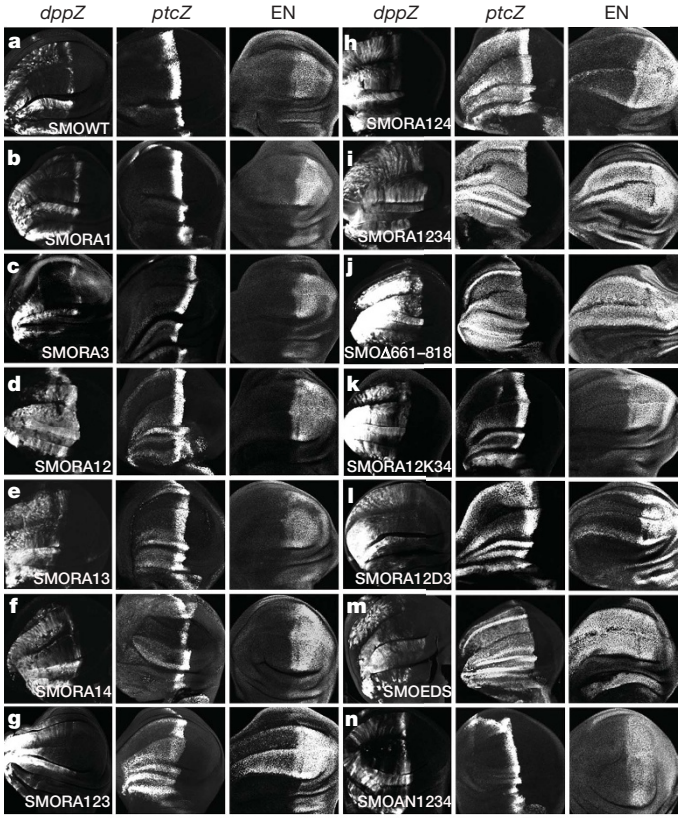

Figure 2 | *In vivo* activities of SMO variants. **a**–**n**, Wing discs expressing the indicated SMO variants from *MS1096* were immunostained to show the expression of *dpp-lacZ* (*dppZ*), *ptc-lacZ* (*ptcZ*) and EN. *dppZ*, *ptcZ* and *en* are induced by low, intermediate and high levels of HH, respectively. The levels of SMO activity inversely correlate with the number of intact Arg clusters (**b**–**i**). An internal deletion removing amino acids 661–818 resulted in high levels of constitutive SMO activity (**j**). SMORA12K34 (**k**) has similar activity to SMORA12 (compare to **d**). SMORA12D3 (**l**) exhibited constitutive activity similar to that of SMORA124 (**h**). **m**, Substitution of the three PKA/CKI phosphorylation clusters with acidic clusters led to high constitutive activity similar to that of SMOSD123 (ref. 15). **n**, SMOAN1234 (see Fig. 4a) did not exhibit higher basal activity than SMOWT (compare to **a**).

we employed fluorescence resonance energy transfer (FRET) analysis, which measures the transfer of energy between yellow fluorescent protein (YFP) and cyan fluorescent protein (CFP) as a function of distance[20]. We initially constructed two pairs of tagged SMO with CFP/YFP either fused to the C terminus (SMO–CFP^C/SMO–YFP^C) or inserted at an amino-terminal position (SMO–CFP^N/SMO–YFP^N) of SMO (Fig. 3a, b; Supplementary Fig. 3). As controls, we constructed CFP/YFP-tagged forms of frizzled 2 (FZ2) and RAB5.

Consistent with a previous finding that FZ family members form constitutive dimers/oligomers[21], we observed high FRET between FZ2–CFP^C/FZ2–YFP^C ($17.3 \pm 1.9\%$) or FZ2–CFP^N/FZ2–YFP^N ($12.6 \pm 1.1\%$) in S2 cells (Fig. 3c, d). Under similar conditions, FRET between SMO–CFP^N/SMO–YFP^N (referred to as $FRET^N$) was $14.1 \pm 1.4\%$ (Fig. 3c), whereas FRET between SMO–CFP^C/SMO–YFP^C ($FRET^C$) was $5.7 \pm 1.3\%$ (Fig. 3d). HH stimulation significantly increased $FRET^C$ to $21.7 \pm 1.5\%$ (Fig. 3d), but only modestly increased $FRET^N$ (Fig. 3c). FRET between control pairs (SMO/FZ2 or SMO/RAB5) was $\leq 1.0\%$ (Fig. 3c, d). In addition, CFP- and YFP-tagged SMO colocalized whereas SMO–CFP barely overlapped with FZ2–YFP (Supplementary Fig. 4). Even in S2 cells stimulated with HH, in which SMO accumulated on the cell surface and overlapped with FZ2, FRET between SMO/FZ2 remained low (Fig. 3c, d, and Supplementary Fig. 4). Furthermore, over fourfold changes in SMO signal intensity did not significantly affect $FRET^C$ (Supplementary Fig. 5).

In wing discs, $FRET^N$ was high in both A and P compartments regardless of HH (Fig. 3e), whereas $FRET^C$ in A-compartment cells distant from the A/P boundary was relatively low but increased significantly in P-compartment cells and in A-compartment cells exposed to HH or lacking PTC (Fig. 3f; Supplementary Figs 6–7a). The high basal $FRET^N$ suggests that SMO forms a constitutive dimer/oligomer (dimer is used hereafter for simplicity), as is the case for the FZ family. Constitutive SMO dimerization was confirmed by immunoprecipitation assays (Supplementary Figs 8 and 9). SMO dimerization is likely to be mediated by SMON, which includes the N-terminal extracellular domain and transmembrane helices, because SMON–CFP^N and SMON–YFP^N colocalized and produced high basal FRET (Fig. 3c).

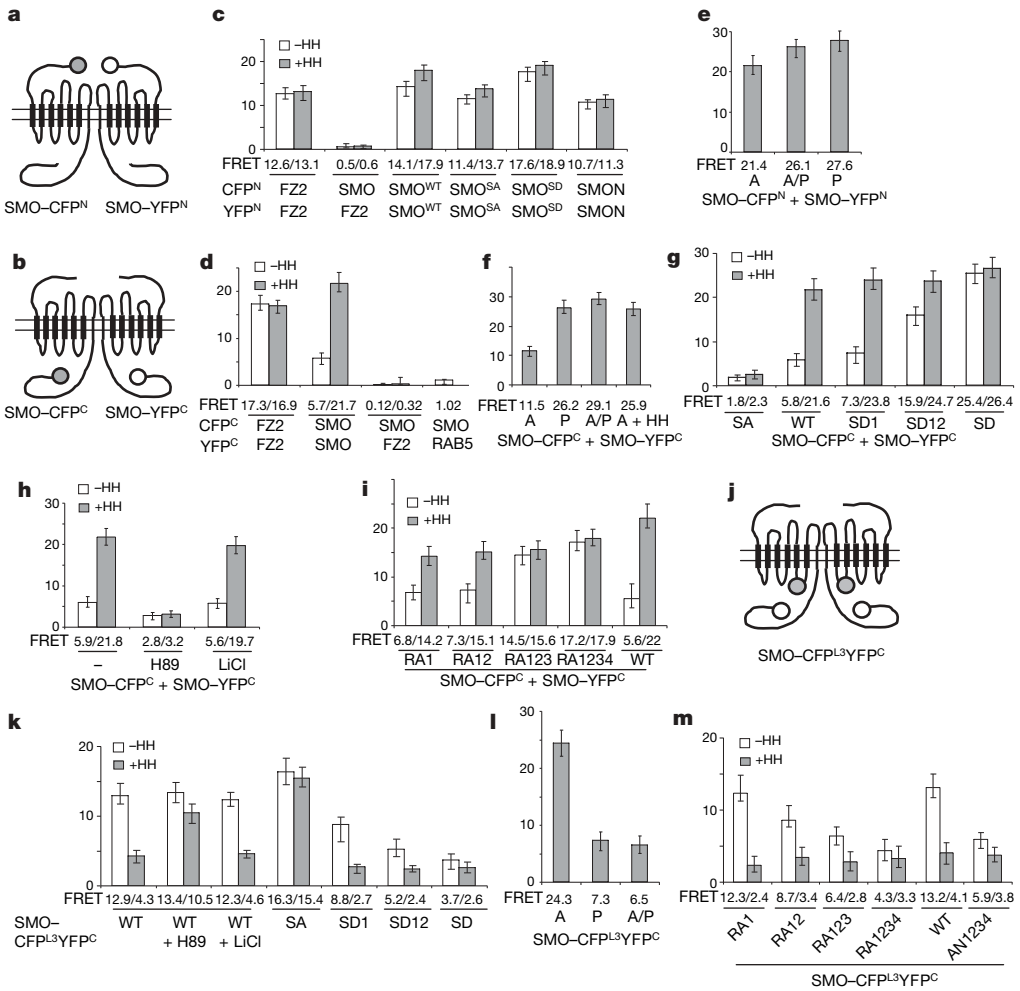

Figure 3 | Regulation of both conformation and proximity of SMO cytoplasmic tails. **a**, **b**, **j**, Cartoons of SMO–CFP^N/SMO–YFP^N (**a**), SMO–CFP^C/SMO–YFP^C (**b**), and SMO–$CFP^{L3}YFP^C$ dimers (**j**). The filled and open circles indicate CFP and YFP, respectively. **c**, **d**, **g**–**i**, **k**, **m**, FRET efficiency (*y* axis and numbers below bars) from the indicated CFP/YFP-tagged constructs in S2 cells treated with or without HH-conditioned medium, and with or without PKA inhibitor H89 or GSK3 inhibitor LiCl (mean ± s.d., $n \geq 10$). SMO^{SA} has three PKA sites mutated to Ala, whereas SMO^{SD1}, SMO^{SD12} and SMO^{SD} have PKA and CKI sites in one, two and three phosphorylation clusters converted to Asp, respectively (**c**, **g**, **k**; ref. 15). SMON lacks a cytoplasmic tail (**c**). RA1, RA12, RA123 and RA1234 have one, two, three and four Arg clusters mutated to Ala, respectively (**i**, **m**; see Fig. 1d). AN1234 has four C-terminal acidic clusters mutated to Ala (**m**; see Fig. 4a). HH increased $FRET^C$ between SMO–CFP^C/SMO–YFP^C (**d**) and decreased $FRET^{L3C}$ from SMO–$CFP^{L3}YFP^C$ (**k**), both of which were blocked by the SA mutations (**g**) or H89 but not by LiCl (**h**, **k**). Phospho-mimetic or RA mutations progressively increased basal $FRET^C$ (**g**, **i**) whereas they gradually decreased $FRET^{L3C}$ (**k**, **m**). **e**, **f**, **l**, FRET efficiency between SMO–CFP^N/SMO–YFP^N (**e**), SMO–CFP^C/SMO–YFP^C (**f**), or from SMO–$CFP^{L3}YFP^C$ (**l**) expressed in wing discs (mean ± s.d., $n \geq 5$). A, A-compartment cells away from the A/P boundary; P, P-compartment cells; A/P, A-compartment cells adjacent to the A/P boundary; A + HH, A-compartment cells expressing *UAS-HH*.

The low basal but high HH-induced $FRET^{C}$ suggests that the two SMO cytoplasmic tails within a dimer are separated from each other but HH signalling increases their proximity. To investigate whether increased proximity is accompanied by a conformational change, we generated a doubly tagged SMO (SMO–$CFP^{L3}YFP^{C}$) with CFP inserted into the third intracellular loop (L3) and YFP fused to the C terminus (Fig. 3j; Supplementary Fig. 3). SMO–$CFP^{L3}YFP^{C}$ responded to HH and possessed signalling activity (Supplementary Figs 10, 11). In S2 cells, basal FRET from SMO–$CFP^{L3}YFP^{C}$ (referred to as $FRET^{L3C}$) was 12.9 ± 1.2% but dropped to 4.3 ± 0.8% after HH treatment (Fig. 3k; Supplementary Fig. 11). In wing discs, $FRET^{L3C}$ was 24.3 ± 2.1% in A-compartment cells distant from the A/P boundary, but dropped to 6.5 ± 1.5% in A-compartment cells near the A/P boundary or to 7.3 ± 1.6% in P-compartment cells (Fig. 3l; Supplementary Fig. 12). $FRET^{L3C}$ also reduced to 5.9 ± 1.2% in A-compartment *ptc* mutant clones (Supplementary Fig. 7b). The high basal $FRET^{L3C}$ is probably due to close proximity between the C terminus and L3 of the same SMO molecule (Supplementary Fig. 13). These results suggest that SMO adopts a closed inactive conformation with its C terminus in close proximity to L3, in quiescent cells. HH promotes SMO to adopt an open active conformation in which its C terminus moves away from L3 but closer to the C terminus of its binding partner.

Phosphorylation regulates SMO conformation

To determine if conformational change and increased proximity of SMO cytoplasmic tails is regulated by phosphorylation, we mutated three PKA sites (Ser 667, Ser 687 and Ser 740) to Ala (SA) or substituted them and adjacent CKI sites with Asp (SD123 or SD for simplicity)[15]. The HH-induced increase in $FRET^{C}$ or decrease in $FRET^{L3C}$ was blocked by the SA mutation as well as a PKA inhibitor H89 (Fig. 3g, h, k), whereas the SD123 substitution resulted in high basal $FRET^{C}$ but low basal $FRET^{L3C}$ (Fig. 3g, k). In contrast, neither the basal nor the HH-induced $FRET^{N}$ was significantly affected by the SA or SD123 mutation (Fig. 3c), suggesting that constitutive SMO dimerization is not regulated by phosphorylation, but conformational change and increased proximity of SMO cytoplasmic tails are triggered by phosphorylation. Mutating multiple Arg clusters also resulted in high basal $FRET^{C}$ but low basal $FRET^{L3C}$ (Fig. 3i, m), suggesting that the Arg motifs keep SMO cytoplasmic tails in a closed inactive conformation.

To assess direct physical interaction between SMO cytoplasmic tails and its regulation by phosphorylation, we applied the CytoTrap yeast two-hybrid assay (Methods Summary). Wild-type SMO cytoplasmic tail ($SMOC^{WT}$) failed to self-associate, whereas phosphomimetic SMO cytoplasmic tail ($SMOC^{SD}$) could self-associate and also interact weakly with SMO^{WT} (Supplementary Fig. 14), indicating that phosphorylation of the SMO cytoplasmic tail may promote self-association.

Our previous study suggests that graded SMO activities are governed by SMO phosphorylation levels[15]. To determine if increasing SMO phosphorylation could induce gradual changes in SMO conformation, we compared $FRET^{C}$ and $FRET^{L3C}$ for several phosphorylation-mimetic forms of SMO. SMO^{SD1}, SMO^{SD12} and SMO^{SD} contain Ser to Asp substitution in one, two and three phosphorylation clusters, respectively, and exhibit progressively higher levels of basal activity[15]. Interestingly, they also exhibited a progressive increase in basal $FRET^{C}$ (Fig. 3g) and gradual decrease in basal $FRET^{L3C}$ (Fig. 3k). Furthermore, $FRET^{C}$ progressively increased, whereas $FRET^{L3C}$ gradually decreased, when increasingly more Arg clusters were mutated (Fig. 3i, m). Thus, increasing SMO phosphorylation seems to induce progressive changes in SMO conformation by antagonizing the Arg clusters. SMO may adopt a series of conformational states determined by its phosphorylation levels. Alternatively, SMO may switch in equilibrium between two distinct conformational states: a closed inactive conformation and an open active conformation; phosphorylation increases the probability for individual SMO to adopt the open active conformation.

Arg clusters mediate intramolecular interaction

To determine how Arg clusters keep SMO in a closed inactive conformation, we tested the possibility that they might be involved in intramolecular interactions. A glutathione *S*-transferase (GST) fusion protein (GST–SMO656–755) that contains the SMO region between amino acids 656–755 (referred to hereafter as SAID for SMO auto-inhibitory domain) was tested for interaction with a set of C-terminal fragments, and a minimal SAID interacting fragment (NT860) was identified that contains the C-terminal region between amino acids 860–1035 (Supplementary Fig. 15). SAID–NT860 interaction was diminished by PKA/CKI phosphorylation as well as RA or SD123 mutations (Fig. 4b, c), and the binding affinity gradually decreased with more phosphorylation or Arg clusters mutated (Fig. 4d). The importance of Arg clusters in the SAID–NT860 interaction indicates that the association may be mediated by electrostatic interactions. Indeed, mutating several acidic clusters in the C-terminal half of NT860 gradually diminished the SAID–NT860 interaction (Fig. 4a, e).

The electrostatic interaction between NT860 and SAID may result in a folding back of the SMO cytoplasmic tail to form a closed conformation (Fig. 4f). Consistently, mutating the acidic clusters (SMOAN1234) resulted in decreased basal $FRET^{L3C}$ (Fig. 3m). However, unlike RA mutations, which not only caused conformational change but also promoted SMO cell surface accumulation, SMOAN1234 exhibited little if any cell surface expression and did not exhibit high levels of constitutive activity (Fig. 2n), indicating that both cell surface accumulation and conformational change may be critical for SMO activity.

Clustering of the SMO cytoplasmic tail activates the HH pathway

To assess the biological significance of SMO dimerization, we analysed two SMO mutants with point mutations in the N-terminal extracellular domain: SMO^{1A3} is encoded by a hypomorphic allele such that Cys 90 is substituted to Ser; and SMO^{F11} is encoded by a strong allele that changes Cys 155 to Tyr (ref. 22). Both mutations reduced basal as well as HH-induced $FRET^{N}$ and $FRET^{C}$, with SMO^{F11} exhibiting more severe defects (Supplementary Fig. 16). Immunoprecipitation assays indicated that SMO^{1A3} and SMO^{F11} failed to dimerize with SMO^{WT} (Supplementary Fig. 17a). Unlike SMO^{WT}, neither SMO^{1A3} nor SMO^{F11} was phosphorylated in response to HH (Supplementary Fig. 17b). In addition, both SMO^{1A3} and SMO^{F11} lost HH-induced activity (Fig. 5a).

If loss of SMO activity was due to compromised dimerization, restoring dimerization to these mutants should rescue their activities. To test this, we developed an inducible dimerization system by taking advantage of the observation that the mammalian receptor tyrosine kinase EphB2 forms a hetero-tetramer with its ligand ephrin B2 (EB2; also known as Efnb2) to trigger bidirectional signalling[23]. Accordingly, we constructed EB2–SMO chimaeric proteins in which the extracellular domain of EB2 was inserted into the SMO N-terminal extracellular domain (Supplementary Fig. 3). When expressed in cl-8 cells, EB2–SMO^{1A3} and EB2–SMO^{F11} failed to be activated by HH-conditioned medium; however, they were activated when cells were exposed to the soluble pre-clustered EphB2 extracellular domain, EphB2-Fc (Fig. 5a). In addition, $FRET^{C}$ between mutant pairs of EB2–SMO–CFP^{C}/EB2–SMO–YFP^{C} increased significantly in response to EphB2-Fc but not HH (Fig. 5b).

To determine if dimerization of the SMO cytoplasmic tail suffices to activate the HH pathway, we constructed EB2–SMO cytoplasmic-tail chimaeric proteins in which the intracellular domain of EB2 was replaced by the wild-type (EB2–$SMOC^{WT}$), phosphorylation-deficient (EB2–$SMOC^{SA}$), or phosphorylation-mimetic (EB2–$SMOC^{SD}$) SMO cytoplasmic tail (Fig. 5e, and Supplementary Fig. 3). In both cl-8 cells and wing discs, EB2–$SMOC^{WT}$ exhibited low

basal activity but was markedly stimulated by EphB2 (Fig. 5c, f). Furthermore, EB2–SMOC^{WT} activated the HH pathway independent of endogenous SMO (Supplementary Fig. 18). EB2–SMOC^{WT} also induced FU phosphorylation in response to EphB2-Fc (Supplementary Fig. 19a). In addition, FRET between EB2–SMOC^{WT}–CFP^{C}/EB2–SMOC^{WT}–YFP^{C} increased significantly in response to EphB2-Fc (Fig. 5d).

EB2–SMOC^{SA} did not significantly activate any HH target genes even after clustering by EphB2 (Fig. 5c, f). PKA-site mutation may lock the cytoplasmic tails in a closed inactive conformation that prevents their association. Consistent with this model, FRET between EB2–SMOC^{SA}–CFP^{C}/EB2–SMOC^{SA}–YFP^{C} remained low after EphB2-Fc treatment (Fig. 5d). EphB2-Fc treatment induced phosphorylation of EB2–SMOC, which was abolished by the SA mutation and H89 (Supplementary Fig. 19b), suggesting that EphB2/EB2-induced clustering of SMO cytoplasmic tails promoted their phosphorylation and close proximity, leading to HH pathway activation.

EB2–SMOC^{SD} exhibited high basal activity, yet its activity was further enhanced by EphB2 (Fig. 5c, f). In addition, FRET between EB2–SMOC^{SD}–CFP^{C}/EB2–SMOC^{SD}–YFP^{C} increased after EphB2-Fc treatment (Fig. 5d). Thus, even though 'phosphorylated' SMO cytoplasmic tails may adopt an open conformation that allows them to interact more avidly, as suggested by their high basal FRET^{C} (Fig. 5d), EphB2/EB2-induced clustering further increased their proximity, leading to enhanced pathway activation. These results further underscore the importance of close proximity between SMO cytoplasmic tails for pathway activation.

Regulation of mammalian SMO

In response to SHH and PTC inactivation, mammalian SMO (Smo) translocates to primary cilia, which is thought to trigger pathway activation[24–26]. To determine if SHH may also regulate Smo conformation, we constructed C- or N-terminally CFP/YFP-tagged Smo or a doubly tagged Smo with CFP inserted into the second intracellular loop (L2) and YFP fused to the C terminus (Supplementary Fig. 20a). All tagged forms exhibited activities similar to that of the untagged wild-type form (Supplementary Fig. 20b). Like *Drosophila* SMO, Smo also exhibited high basal FRET^{N} and low basal FRET^{C}; however, SHH as well as an oncogenic mutation (A1)[27] induced significant increases in FRET^{C} (Supplementary Fig. 20c, d). In addition, both SHH and the A1 mutation reduced FRET from Smo–CFP^{L2}YFP^{C} (FRET^{L2C}; Supplementary Fig. 20e), indicating that Smo may also exist as a constitutive dimer and that SHH induces a conformational change, leading to increased proximity of Smo cytoplasmic tails. Interestingly, induced clustering of full-length Smo through the ephrin B2/EphB2 system also triggered pathway activation; however, unlike *Drosophila* SMO, clustering of Smo cytoplasmic tails failed to activate the pathway (Supplementary Fig. 21). It is possible that other intracellular domains such as L3 may be essential for inducing the active conformation of Smo and/or recruiting the intracellular signalling complex because point mutations in L3 inactivate Smo[28].

Vertebrate SMO proteins contain multiple conserved clusters of basic residues in their cytoplasmic tails, including a long stretch of Arg/Lys residues in the central region (Supplementary Fig. 22a). Interestingly, mutating this long stretch of Arg/Lys residues to Ala resulted in constitutive activity of Smo, increased FRET^{C} and decreased FRET^{L2C} (Supplementary Fig. 22b–e), indicating that Smo may employ an Arg/Lys cluster to regulate its conformation and activity.

Discussion

The prevalent view regarding SMO regulation is that SMO is activated as a result of subcellular compartmentation[14,15,24–26,29]. Here we

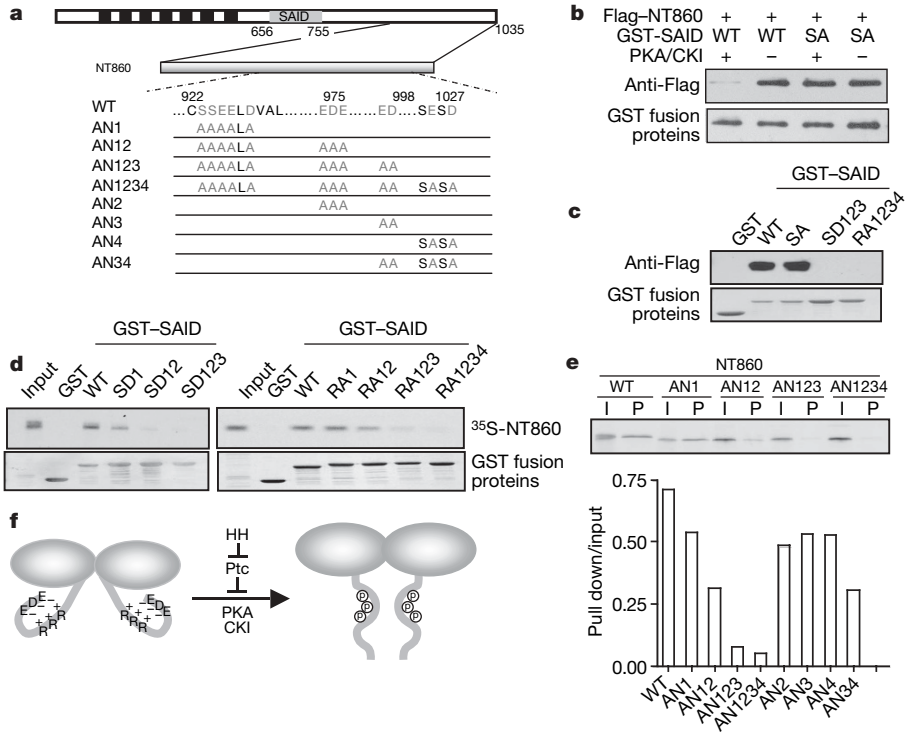

Figure 4 | The Arg clusters mediate intramolecular electrostatic interaction. **a**, Diagram of SMO with the SAID indicated by a grey box, and NT860 with indicated substitutions. **b**, GST pull-down assay using GST–SAID and S2 cell extracts expressing the indicated Flag-tagged SMO C-terminal fragments. **c**, **d**, GST pull-down experiments using wild-type or the indicated mutant GST–SAID and S2 cell extracts expressing Flag-tagged NT860 (**c**) or *in vitro* translated ^{35}S-labelled NT860 (**d**). **e**, Autoradiography (upper panel) and quantification (lower panel) of a GST pull-down assay using GST–SAID and *in vitro* translated ^{35}S-labelled wild-type (WT) or mutant (AN) NT860. I, input; P, pulled-down protein. The binding affinity was indicated by the ratio of pulled-down protein (pull down) to input. **f**, A model for regulating SMO conformation by multiple Arg clusters and HH-induced phosphorylation; see text for detail.

provide substantial evidence that SMO activity is also regulated by a conformational switch. In particular, we identified an autoinhibitory domain (SAID) in the *Drosophila* SMO cytoplasmic tail, containing multiple Arg clusters that keep SMO in a closed inactive conformation through intracellular electrostatic interaction (Fig. 4f). HH-induced phosphorylation disrupts such interaction and triggers a conformational switch and increased proximity of SMO cytoplasmic tails, which may further promote recruitment and interaction of intracellular signalling complexes[30–33]. Our results also indicate that the Arg clusters may promote endocytosis and degradation of SMO, whereas multiple phosphorylation events neutralize the negative effect of the Arg clusters either by inhibiting endocytosis and/or promoting recycling of SMO.

A striking feature of the SAID domain is that it contains multiple regulatory modules each of which consists of an Arg cluster linked to a phosphorylation cluster. The pairing of positive and negative regulatory elements may offer precise regulation, because phosphorylation at a given cluster may only neutralize adjacent negative element(s), leading to an incremental change in SMO activity. We propose that increasing phosphorylation gradually neutralizes the negative effect of multiple Arg clusters, leading to a progressive increase in SMO cell surface expression and activity (Supplementary Fig. 23). Thus, by employing multiple Arg clusters as inhibitory elements that are counteracted by differential phosphorylation, SMO acts as a rheostat to translate graded HH signals into distinct responses.

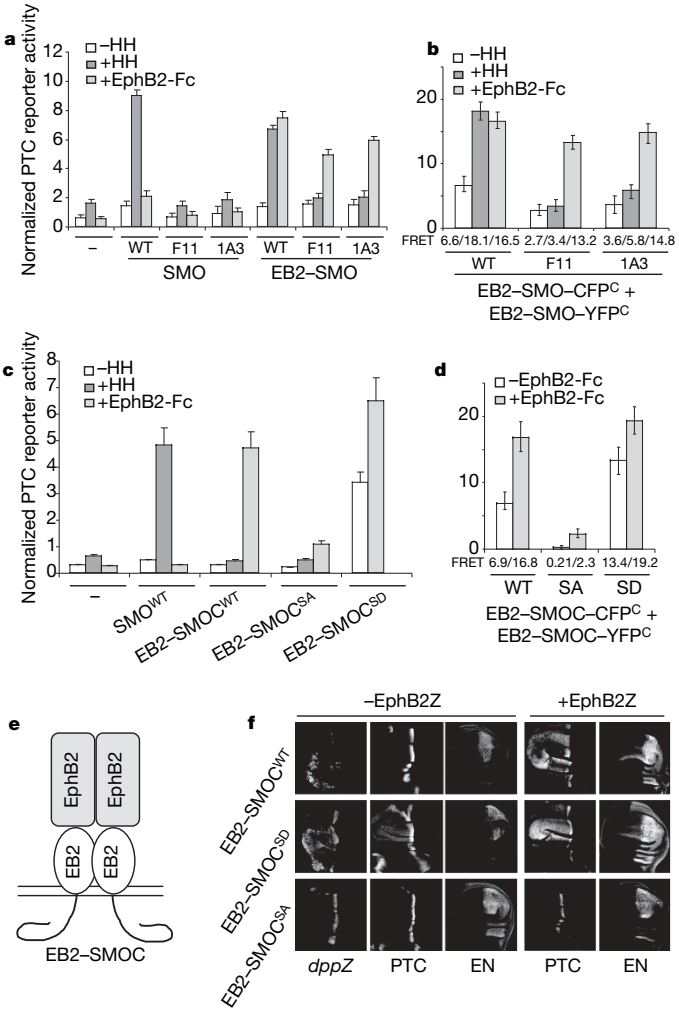

Figure 5 | Clustering of SMO cytoplasmic tails triggers HH pathway activation. a, **c**, The *ptc-luc* reporter assay in cl-8 cells transfected with the indicated SMO expression constructs and treated with or without HH-conditioned medium or EphB2-Fc. Error bars, 1 s.d. (triplicate wells). **b**, **d**, FRET between wild-type or mutant pairs of EB2–SMO–CFP^C/EB2–SMO–YFP^C (**b**) or EB2–SMOC–CFP^C/EB2–SMOC–YFP^C (**d**) expressed in S2 cells treated with or without HH-conditioned medium or EphB2-Fc (mean ± s.d., $n \geq 10$). **e**, Cartoon of the EB2–SMOC–EphB2 complex. **f**, Wing discs expressing the indicated SMO constructs with or without EphB2Z under the control of the *MS1096 Gal4* driver were immunostained to show the expression of *dpp-lacZ* (*dppZ*), PTC and EN. Of note, EB2–$SMOC^{SD}$ exhibited higher basal activity than EB2–$SMOC^{WT}$ because it induced higher levels of ectopic *dppZ* and also induced ectopic albeit low levels of *ptc*. When coexpressed with EphB2Z, both EB2–$SMOC^{WT}$ and EB2–$SMOC^{SD}$ ectopically activated high levels of *ptc* and low levels of *en*. In contrast, EB2–$SMOC^{SA}$ failed to activate any HH target genes.

METHODS SUMMARY

smo^3 and *ptc*^{IIW} are strong alleles of *smo* and *ptc*, respectively (http://flybase.bio.indiana.edu/). *MS1096*, *ptc-Gal4*, *dpp-lacZ*, *UAS-smo–*CFP^C*/UAS-smo–*YFP^C and their mutant derivatives have been described[15]. *Drosophila smo* and mouse *Smo* constructs were generated using the *pUAST* and *pGE* vectors, respectively. Amino acid substitutions were generated using PCR-based mutagenesis. Fly transformants were generated by standard P-element mediated transformation. Multiple independent transgenic lines were tested for activity. Immunostaining was carried out as described[34]. S2 and cl-8 cells were cultured as described[35,36]. Treatment of transfected cells with HHN-conditioned medium and *ptc-luc* reporter assays were carried out as described[32]. Cell surface staining was carried out as described[15]. NIH-3T3 cells were cultured in DMEM medium. Mammalian reporter assays were performed essentially as described[27]. For GST pull-down assays, S2 cell lysates or reticulocytes with *in vitro* translated ^{35}S-labelled proteins were incubated with GST fusion proteins absorbed on glutathione beads. Proteins bound to the beads were separated on SDS–PAGE, followed by western blot or autoradiography. Immunoprecipitation and western blot analysis were carried out using standard protocols. Yeast two-hybrid assays were carried out using Stratagene's CytoTrap system according to the manufacturer's instructions. For FRET analysis, a Zeiss LSM510 confocal microscope was used. CFP was excited at 458 nm wavelength and the emission was collected through a BP 480–520 nm filter. YFP was excited at 514 nm wavelength and the emission was collected through a BP 535–590 nm filter. CFP signal was obtained once before (BP) and once after (AP) photobleaching YFP using the full power of the 514 nm laser line for 1–2 min at the top half of each cell or selected disc area, leaving the bottom as an internal control. The intensity change of CFP was analysed using the Metamorph software (Universal Imaging). The efficiency of FRET was calculated using the formula: FRET% = $[(CFP_{AP} - CFP_{BP})/CFP_{AP}] \times 100$.

Full Methods and any associated references are available in the online version of the paper at www.nature.com/nature.

Received 4 June; accepted 7 September 2007.
Published online 24 October 2007.

1. Ingham, P. W. & McMahon, A. P. Hedgehog signaling in animal development: paradigms and principles. *Genes Dev.* **15,** 3059–3087 (2001).
2. Heemskerk, J. & DiNardo, S. *Drosophila* hedgehog acts as a morphogen in cellular patterning. *Cell* **76,** 449–460 (1994).
3. Roelink, H. *et al.* Floor plate and motor neuron induction by different concentrations of the amino-terminal cleavage product of sonic hedgehog autoproteolysis. *Cell* **81,** 445–455 (1995).
4. Riddle, R. D., Johnson, R. L., Laufer, E. & Tabin, C. *Sonic hedgehog* mediates the polarizing activity of the ZPA. *Cell* **75,** 1401–1416 (1993).
5. Hooper, J. E. & Scott, M. P. Communicating with Hedgehogs. *Nature Rev. Mol. Cell Biol.* **6,** 306–317 (2005).
6. Jia, J. & Jiang, J. Decoding the Hedgehog signal in animal development. *Cell. Mol. Life Sci.* **63,** 1249–1265 (2006).
7. Basler, K. & Struhl, G. Compartment boundaries and the control of *Drosophila* limb pattern by *hedgehog* protein. *Nature* **368,** 208–214 (1994).
8. Tabata, T. & Kornberg, T. B. Hedgehog is a signaling protein with a key role in patterning *Drosophila* imaginal discs. *Cell* **76,** 89–102 (1994).
9. Strigini, M. & Cohen, S. M. A Hedgehog activity gradient contributes to AP axial patterning of the *Drosophila* wing. *Development* **124,** 4697–4705 (1997).
10. van-den-Heuval, M. & Ingham, P. W. *smoothened* encodes a receptor-like serpentine protein required for *hedgehog* signalling. *Nature* **382,** 547–551 (1996).
11. Alcedo, J., Ayzenzon, M., Von Ohlen, T., Noll, M. & Hooper, J. E. The *Drosophila smoothened* gene encodes a seven-pass membrane protein, a putative receptor for the Hedgehog signal. *Cell* **86,** 221–232 (1996).
12. Chen, Y. & Struhl, G. Dual roles for Patched in sequestering and transducing Hedgehog. *Cell* **87,** 553–563 (1996).
13. Stone, D. M. *et al.* The tumour-suppressor gene *patched* encodes a candidate receptor for Sonic hedgehog. *Nature* **384,** 129–134 (1996).

14. Denef, N., Neubuser, D., Perez, L. & Cohen, S. M. Hedgehog induces opposite changes in turnover and subcellular localization of patched and smoothened. *Cell* **102,** 521–531 (2000).
15. Jia, J., Tong, C., Wang, B., Luo, L. & Jiang, J. Hedgehog signalling activity of smoothened requires phosphorylation by protein kinase A and casein kinase I. *Nature* **432,** 1045–1050 (2004).
16. Zhang, C., Williams, E. H., Guo, Y., Lum, L. & Beachy, P. A. Extensive phosphorylation of Smoothened in Hedgehog pathway activation. *Proc. Natl Acad. Sci. USA* **101,** 17900–17907 (2004).
17. Apionishev, S., Katanayeva, N. M., Marks, S. A., Kalderon, D. & Tomlinson, A. *Drosophila* Smoothened phosphorylation sites essential for Hedgehog signal transduction. *Nature Cell Biol.* **7,** 86–92 (2005).
18. Schlessinger, J. Cell signaling by receptor tyrosine kinases. *Cell* **103,** 211–225 (2000).
19. Bourne, H. R. How receptors talk to trimeric G proteins. *Curr. Opin. Cell Biol.* **9,** 134–142 (1997).
20. Centonze, V. E., Sun, M., Masuda, A., Gerritsen, H. & Herman, B. Fluorescence resonance energy transfer imaging microscopy. *Methods Enzymol.* **360,** 542–560 (2003).
21. Kaykas, A. *et al.* Mutant Frizzled 4 associated with vitreoretinopathy traps wild-type Frizzled in the endoplasmic reticulum by oligomerization. *Nature Cell Biol.* **6,** 52–58 (2004).
22. Nakano, Y. *et al.* Functional domains and sub-cellular distribution of the Hedgehog transducing protein Smoothened in *Drosophila*. *Mech. Dev.* **121,** 507–518 (2004).
23. Himanen, J. P. & Nikolov, D. B. Eph signaling: a structural view. *Trends Neurosci.* **26,** 46–51 (2003).
24. Huangfu, D. & Anderson, K. V. Signaling from Smo to Ci/Gli: conservation and divergence of Hedgehog pathways from *Drosophila* to vertebrates. *Development* **133,** 3–14 (2006).
25. Corbit, K. C. *et al.* Vertebrate Smoothened functions at the primary cilium. *Nature* **437,** 1018–1021 (2005).
26. Rohatgi, R., Milenkovic, L. & Scott, M. P. Patched1 regulates hedgehog signaling at the primary cilium. *Science* **317,** 372–376 (2007).
27. Taipale, J. *et al.* Effects of oncogenic mutations in Smoothened and Patched can be reversed by cyclopamine. *Nature* **406,** 1005–1009 (2000).
28. Varjosalo, M., Li, S. P. & Taipale, J. Divergence of hedgehog signal transduction mechanism between *Drosophila* and mammals. *Dev. Cell* **10,** 177–186 (2006).
29. Zhu, A. J., Zheng, L., Suyama, K. & Scott, M. P. Altered localization of *Drosophila* Smoothened protein activates Hedgehog signal transduction. *Genes Dev.* **17,** 1240–1252 (2003).
30. Jia, J., Tong, C. & Jiang, J. Smoothened transduces Hedgehog signal by physically interacting with Costal2/Fused complex through its C-terminal tail. *Genes Dev.* **17,** 2709–2720 (2003).
31. Ruel, L., Rodriguez, R., Gallet, A., Lavenant-Staccini, L. & Therond, P. P. Stability and association of Smoothened, Costal2 and Fused with Cubitus interruptus are regulated by Hedgehog. *Nature Cell Biol.* **5,** 907–913 (2003).
32. Lum, L. *et al.* Hedgehog signal transduction via Smoothened association with a cytoplasmic complex scaffolded by the atypical kinesin, Costal-2. *Mol. Cell* **12,** 1261–1274 (2003).
33. Ogden, S. K. *et al.* Identification of a functional interaction between the transmembrane protein Smoothened and the kinesin-related protein Costal2. *Curr. Biol.* **13,** 1998–2003 (2003).
34. Jiang, J. & Struhl, G. Protein kinase A and Hedgehog signalling in *Drosophila* limb development. *Cell* **80,** 563–572 (1995).
35. Zhang, W. *et al.* Hedgehog-regulated costal2-kinase complexes control phosphorylation and proteolytic processing of cubitus interruptus. *Dev. Cell* **8,** 267–278 (2005).
36. van Leeuwen, F., Harryman Samos, C. & Nusse, R. Biological activity of soluble *wingless* protein in cultured *Drosophila* imaginal disc cells. *Nature* **368,** 342–344 (1994).
37. Dravis, C. *et al.* Bidirectional signaling mediated by ephrin-B2 and EphB2 controls urorectal development. *Dev. Biol.* **271,** 272–290 (2004).

Supplementary Information is linked to the online version of the paper at www.nature.com/nature.

Acknowledgements We thank B. Wang and S. Thet for technical assistance, L. Zhang for assistance with yeast two-hybrid experiments, Q. Shi for help with Smo constructs, M. Chumley, L. Lum, P. Beachy, I. Guerrero and DSHB for reagents, and K. Wharton and H. Kramer for comments. Y.Z. was supported by a National Scientist Development Grant from the American Heart Association. J.J. was supported by grants from the National Institutes of Health, the Leukemia & Lymphoma Society Scholar Program, and the Robert A. Welch Foundation. J.J. is a Eugene McDermott Endowed Scholar of Biomedical Science at UTSW.

Author Contributions Y.Z. and C.T. participated in the design, execution and analysis of experiments, and the preparation of the manuscript. Y.Z. conducted and analysed all the FRET experiments. C.T. identified the Arg clusters. J.J. participated in the design and analysis of experiments and writing the manuscript.

Author Information Reprints and permissions information is available at www.nature.com/reprints. Correspondence and requests for materials should be addressed to J.J. (jin.jiang@utsouthwestern.edu).

METHODS

Constructs and transgenes. SMO C-terminal deletion constructs were generated by PCR amplification of the corresponding coding sequences, followed by subcloning into a *pUAST* vector containing CFP coding sequence so that the CFP was fused to the C terminus of each SMO deletion mutant. For Ala-scan mutagenesis and F11, 1A3, RA, SA and SD mutations, substitutions were generated by PCR-based site-directed mutagenesis. For *UAS-Smo–CFP^{L3}YFP^{C}*, the CFP coding sequence was inserted between SMO amino acids 451–452, and YFP was fused to the C terminus. To construct mutant forms of SMO–CFP^{C}/YFP^{C} or SMO–CFP^{L3}YFP^{C}, the corresponding mutant sequences were swapped by using a unique *Spe*I site in the seventh transmembrane domain. To construct wild-type or mutant forms of SMO–CFP^{N}/YFP^{N}, CFP/YFP was inserted in frame into a unique *Sfi*I site near the N-terminal region. To construct EB2–SMOC chimaerical proteins, the intracellular domain of EB2 was replaced by wild-type or mutant forms of the SMO cytoplasmic tail (amino acids 556–1035). To construct EB2–SMO^{WT}, EB2–SMO^{F11} and EB2–SMO^{A11}, the extracellular domain of EB2 was fused to SMO sequence encoding amino acids 33–1035. EphB2Z contains a full-length EphB2 fused to β-galactosidase to facilitate oligomerization[37]. To generate GST–SMO fusion constructs, *smo* complementary DNA fragments encoding amino acids 656–755 with wild-type sequence or point mutations were amplified by PCR and inserted between *Not*I and *Eco*RI sites in the *pGEX4T-2* vector. To generate Flag-tagged SMO C-terminal fragments such as SMO-NT860, the corresponding cDNA fragments were amplified by PCR and subcloned to a *pUAST-Flag* vector. To construct Smo–CFP^{C}/YFP^{C}, CFP/YFP was fused in frame to the Smo C terminus. To construct Smo–CFP^{N}/YFP^{N}, CFP/YFP was inserted in frame after amino acid 31. To construct Smo–CFP^{L2}YFP^{C}, the CFP coding sequence was inserted between Smo residues 355 and 356, and YFP was fused in frame to the C terminus. For EB2–Smo, the extracellular domain of EB2 was fused N-terminally to the full-length Smo. For EB2–SmoC, the intracellular domain of EB2 was replaced by the Smo cytoplasmic tail (amino acids 544–793). Multiple independent transgenic lines were tested for each construct. *MS1096*, *ptc-gal4*, *dpp-lacZ*, *UAS-smo–CFP^{C}/YFP^{C}* and their mutant derivative have been described[15].

Cell culture, immunoprecipitation, GST pull-down, western blot, immunostaining and luciferase reporter assay. S2 and cl-8 cells were cultured as described[35,36]. Transfection was carried out using the Calcium Phosphate Transfection Kit (Speciality Media). HH-condition medium treatment was carried out as described[32]. Immunoprecipitation and western blot analysis were carried out using standard protocols. For cell surface staining, transfected cells were fixed with 4% paraformaldehyde and incubated with primary antibody in PBS for 30 min at room temperature, followed by incubation with secondary antibody in PBT. For GST pull-down assays, GST fusion proteins absorbed on glutathione beads were washed three times with ice-cold PBS containing 1% NP40. Cell lysates from S2 cells expressing tagged SMO C-terminal fragments or reticulocytes with *in vitro* translated ^{35}S-labelled SMO C-terminal fragments were then added and the mixtures were incubated at 4 °C for 1 h with occasional mixing. Proteins bound to the beads were washed five times with PBS plus 1% NP40 before separation on SDS–PAGE, followed by western blot or autoradiography. For EphB2-Fc treatment, EphB2-Fc chimaera (R&D Systems) and goat anti-human IgG Fc (Jackson Immunoresearch Labs) were mixed for 4 h at 4 °C before being added into cultured cells. NIH-3T3 cells were cultured in DMEM containing 10% bovine calf serum and antibiotics penicillin/streptomycin at 5% CO_2 in a humidified incubator. Transfection of NIH-3T3 cells was carried out using FuGENE6 (Roche). Briefly, after transfection for 2 days, cell culture medium was changed to DMEM with 0.5% bovine calf serum with or without recombinant mouse SHHN (R&D Systems). Mammalian reporter assays were performed essentially as described[27]. Immunostaining of imaginal discs was carried out as described[34]. Antibodies used in this study were: rabbit anti-βGal (Cappel), mouse anti-PTC (from I. Guerrero), mouse anti-EN (DSHB), rabbit and mouse anti-Flag (Sigma), mouse anti-SMON (DSHB) and mouse anti-Myc (Santa Cruz).

FRET analysis using confocal microscopy. For FRET analysis of cultured cells, CFP- and YFP-tagged constructs were transfected into S2 cells together with an *ub-Gal4* expression vector[15]. Transfected cells were treated with or without HH-conditioned medium. For maximal HH signalling strength, a *UAS-HH* expression construct was also included in the transfection[32]. Cells were washed with PBS, fixed with 4% formaldehyde for 20 min, and mounted on slides in 80% glycerol. For FRET analysis of wing discs, *smo* transgenes were expressed with *MS1096* (for analysis of A- or P-compartment cells) or *ptc-Gal4* (for analysis of A-compartment cells near the A/P boundary). Late third instar wing discs were fixed with 4% formaldehyde and mounted on slides in 80% glycerol. Fluorescence signals were acquired with the ×100 objective of a Zeiss LSM510 confocal microscope. Each data set was based on 10–15 individual cells. In each cell, four to five regions of interest in photobleached area were selected for analysis.

Yeast two-hybrid assay. The prey and bait plasmids were constructed using the C-terminal fragment of SMO (amino acids 641–1035).